Monthly Notices
of the
ROYAL ASTRONOMICAL SOCIETY

MNRAS **450,** 3991–3998 (2015) doi:10.1093/mnras/stv906

Multicolour time series photometry of the T Tauri star CVSO 30

C. Koen★

Department of Statistics, University of the Western Cape, Private Bag X17, Bellville, 7535 Cape Town, South Africa

Accepted 2015 April 19. Received 2015 April 14; in original form 2015 February 25

ABSTRACT

Five consecutive runs of at least five hours, and two shorter runs, of $V(RI)_C$ time series photometry of CVSO 30 are presented. No evidence could be seen for planetary transits, previously claimed in the literature for this star. The photometry described in this paper, as well as earlier observations, can be modelled by two non-sinusoidal periodicities of 8 and 10.8 h (frequencies 3 and 2.23 d^{-1}) or their 1 d^{-1} aliases. The possibility is discussed that star-spots at different latitudes of a differentially rotating star is responsible for the brightness modulations. The steep wavelength dependence of the variability amplitudes is best described by hot star-spots.

Key words: stars: individual: CVSO 30 – stars: individual: CVSO 209 – stars: variables: T Tauri, Herbig Ae/Be.

1 INTRODUCTION

The subject of this paper, CVSO 30 (2MASS J05250755+0134243) was discovered to be a variable star by Briceño et al. (2005), in the course of a survey of the Orion OB1 association. (The nomenclature 'CVSO' refers to the 'Centro de Investigaciones de Astronomia' Variability Survey in Orion.) Pertinent observational information from the discovery paper is that the star lies in the slightly older (7–10 Myr) OB1a sub-association; the spectral type is M3; the level of variability observed in the V band was 0.45 mag; and the Hα spectral feature was in emission, with an equivalent width of 11.4 Å. Based on these characteristics CVSO 30 was classified as a weak-lined T Tauri star (WTTS). The following further properties were deduced: $T_{\rm eff} = 3470$ K, $R/{\rm R}_\odot = 1.39$, $0.34 \lesssim M/{\rm M}_\odot \lesssim 0.44$ and an age of 2.63–2.68 Myr. Examination of *Spitzer* photometry by Hernández et al. (2007) did not uncover any evidence of an infrared excess, hence it was concluded that there is no circumstellar disc – which is consistent with the WTTS classification.

Several thousand R-band photometric measurements of CVSO 30 were made by the Palomar Transit Factory (PTF). An extensive analysis of these observations was presented by Van Eyken et al. (2012), who refer to the star also as PTFO 8-8695. The authors found a 0.4484 d period (frequency 2.230 d^{-1}) in their observations, presumably induced by stellar rotation. The non-sinusoidal periodic variations did not repeat exactly from cycle to cycle, and included low-amplitude depressions with durations of ∼1.8 h. Van Eyken et al. (2012) ascribed the dips to planetary transits, caused by a planet with orbital period locked to the stellar rotation period. The 0.4484 d periodicity is somewhat obscured in the light curves by typical aperiodic T Tauri variability. High-resolution spectroscopy ruled out binarity as an explanation for the periodicity, and provided the estimate $v \sin i = 81 \pm 8$ km s^{-1}.

The author is aware of two other sets of time series photometry of CVSO 30. A brief description of the results of monitoring by the 'Young Exoplanet Transit Initiative' can be found in Errmann et al. (2014), while Catalina Sky Survey (CSS; e.g. Drake et al. 2014) observations are publicly available online. The PTF and Catalina data are analysed below, along with the new multifilter time series photometry described in the next section of the paper.

2 THE SAAO OBSERVATIONS

All measurements were made with the SAAO (South African Astronomical Observatory) STE4 CCD camera mounted on the SAAO 1.9-m telescope at Sutherland, South Africa. The field of view of the camera on the telescope is 2.5 × 2.5 arcmin^2. Pre-binning of the images was performed throughout, giving a reasonable readout time of roughly 20 s. Weather permitting, observations were cycled through the $V(RI)_C$ filters – see Table 1 for an observing log. (Note that R and I are Cousins system filters, but that the subscripts will henceforth be omitted for convenience.) All of the observing was done under bright moonlight conditions, mostly with clear sky, but sometimes with poor (>1.5 arcsec) seeing. Since its late spectral type makes the star particularly faint in V, observations were restricted to R and I when conditions were particularly poor. Exposure times ranged from 50 to 70 s in I, 90–120 s in R and 160–200 s in V.

Photometric reductions were performed using an automated version of DOPHOT (Schechter, Mateo & Saha 1993). Magnitudes determined from point spread functions proved considerably less noisy than those from aperture photometry, which was no surprise, given the very high sky background counts. The analysis reported below was performed on differential magnitudes of CVSO 30.

Light curves are plotted in Figs 1–4. (The data in the figures are available electronically on the journal web site as supplementary material). There may be some slight changes in mean light level from night to night, but it seems more likely that the small shifts are due to random variability in the standardization.

★ E-mail: ckoen@uwc.ac.za

Table 1. The observing log. The range in the number of useful measurements (across different filters) is in the last column.

Starting time (HJD 2457020+)	Filters	Run length (h)	*N*
3.3840	*VRI*	2.4	22–24
4.2961	*VRI*	1.0	10
5.2957	*RI*	7.2	81–84
6.2990	*VRI*	6.9	46–66
7.2928	*VRI*	6.6	40–67
8.2862	*VRI*	7.2	58–63
9.2860	*VRI*	5.2	46–48

Amplitudes of variability increase with increasing wavelength, as is the rule in T Tauri stars. The amplitude increase from *I* to *R* is sufficiently sharp as to suggest the presence of hot stellar spots, rather than cool (e.g. Stahler & Palla 2004), but the *V* amplitude, on the other hand, is not that much larger than in *R*. The light curves in Figs 2–4 also generally have the overall sinusoidal appearance typical of the effects of star-spots.

Van Eyken et al. (2012) provide an ephemeris for the posited mid-transit timings. Timings lying within the interval covered by the present observations are listed in Table 2. With the possible exceptions of timings on HJD 2457027 and HJD 2457028, light curves in Figs 2–4 do not appear to support the presence of transits at the predicted times.

It is none the less possible that shallow transits are hidden by more overt variability, an avenue thoroughly explored by Van Eyken et al. (2012). In the following section, the light curves are modelled by a decomposition in terms of sinusoids; the residuals can then be examined for transit signatures.

3 FREQUENCY ANALYSIS OF THE SAAO PHOTOMETRY

Inspection of Fig. 2 shows that the dominant period in the data is at least 6 h (i.e. comparable to the length of the longest run, on HJD 2457025). On the other hand, Fig. 1 shows maxima of similar heights on successive nights, separated by close to a day.

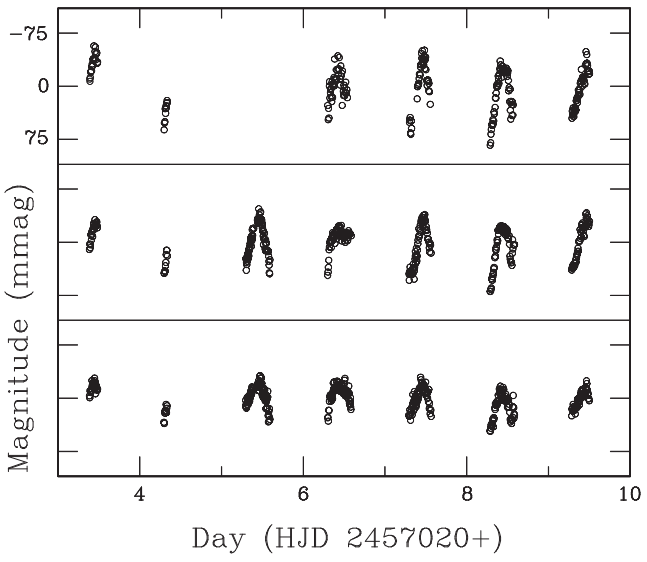

Figure 1. The SAAO observations of CVSO 30 in *V*, *R* and *I* are shown from top to bottom.

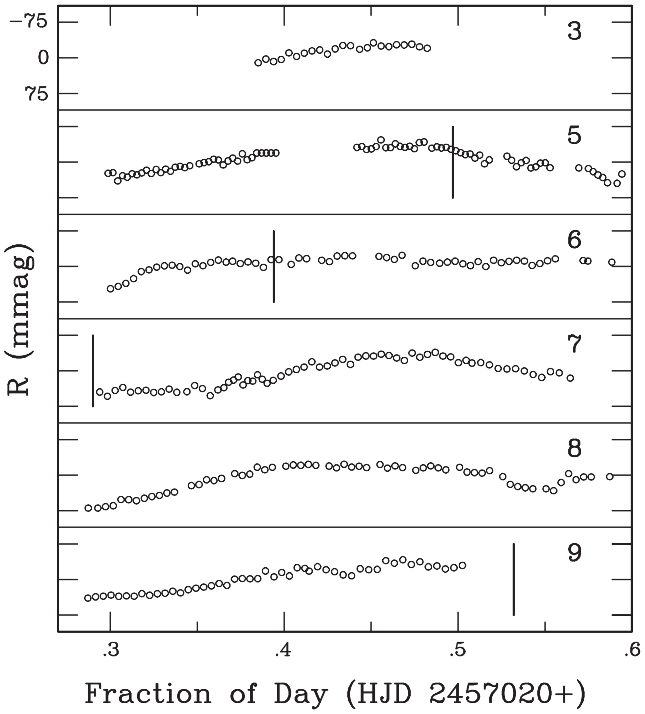

Figure 2. The *R*-band SAAO measurements of CVSO 30. Panels are labelled with the last digit of the Julian Day of observation. Note that the light-curve maxima are reached at similar times every night, i.e. there is a periodicity of roughly 24 h (or a sub-multiple thereof) in the data. Vertical lines in the panels indicate predicted times of planetary mid-transits (Table 2).

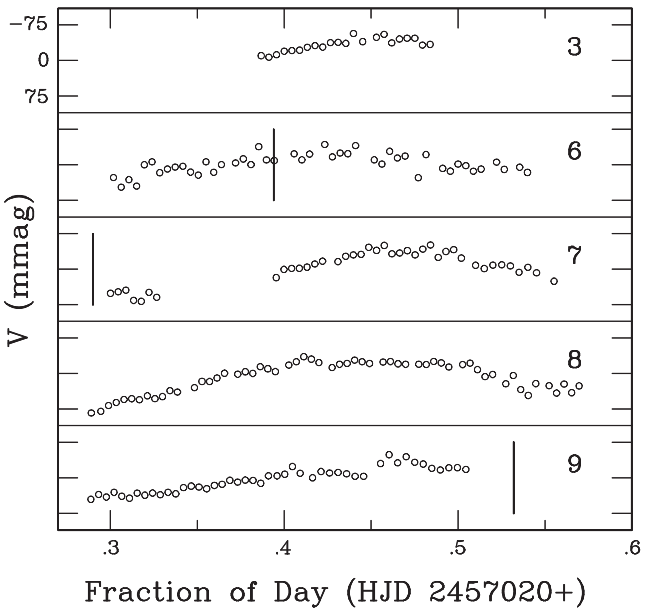

Figure 3. As for Fig. 2, but for the *V* band.

The implication is that the major periodicity is approximately a day, or a sub-multiple of a day, i.e. ∼6, 8, 12 or 24 h.

The visual impression is confirmed by the amplitude spectra in Fig. 5. The 1 d^{-1} aliasing pattern shows peaks in the range ∼2–5 d^{-1}, with the most plausible being 3 or 4 d^{-1}. Frequencies corresponding to the highest peaks are given in the first line of Table 3. Amplitudes listed in the table were obtained by linear least-squares fitting of

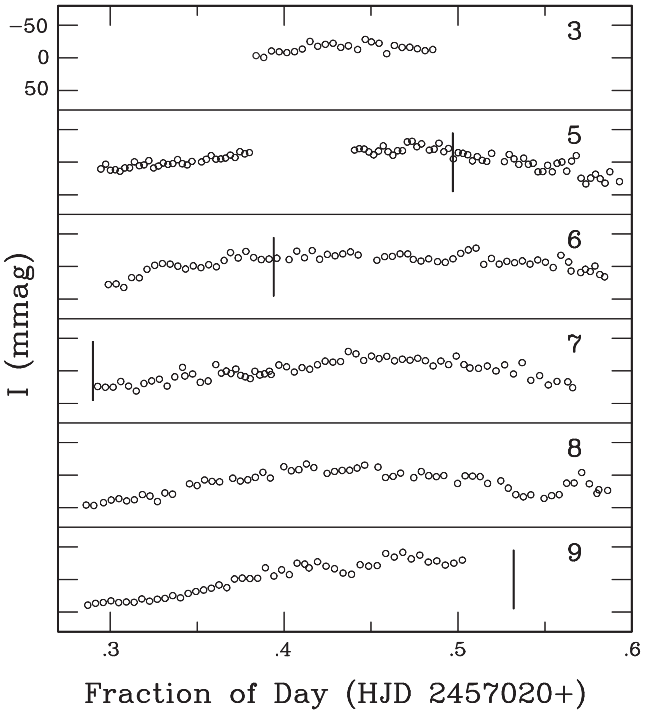

Figure 4. As for Fig. 2, but for the *I* band.

Table 2. Times of mid-transit, predicted from the ephemeris $T = 245\,5543.9402 + 0.448\,413E$ (van Eyken et al. 2012).

E	*T*	*E*	*T*	*E*	*T*
3299	3.255	3305	5.945	3311	8.636
3300	3.703	3306	6.394	3312	9.084
3301	4.152	3307	6.842	3313	9.532
3302	4.600	3308	7.290	3314	9.981
3303	5.048	3309	7.739	–	–
3304	5.497	3310	8.187	–	–

sinusoids to the data: values range from 34 mmag in *V* to 16 mmag in *I*.

The fitted sinusoids were pre-whitened from the data, and spectra of the residuals were calculated – see Fig. 6 for the results. Maximal amplitudes are at the level of about 10 mmag, or below. Continuing the pre-whitening until five sinusoids have been removed from each of the three data sets gives rise to the spectra in Fig. 7. The only features of note are the largest peaks in the *V* and *R* residuals, at frequencies 8.94 and 8.89 d^{-1}, respectively.

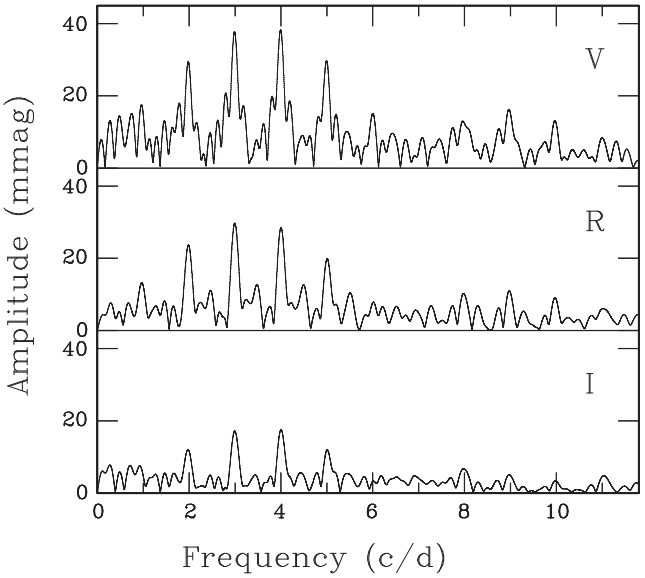

Figure 5. Amplitude spectra of the data in Figs 2–4. Note the strong wavelength dependence of the amplitudes.

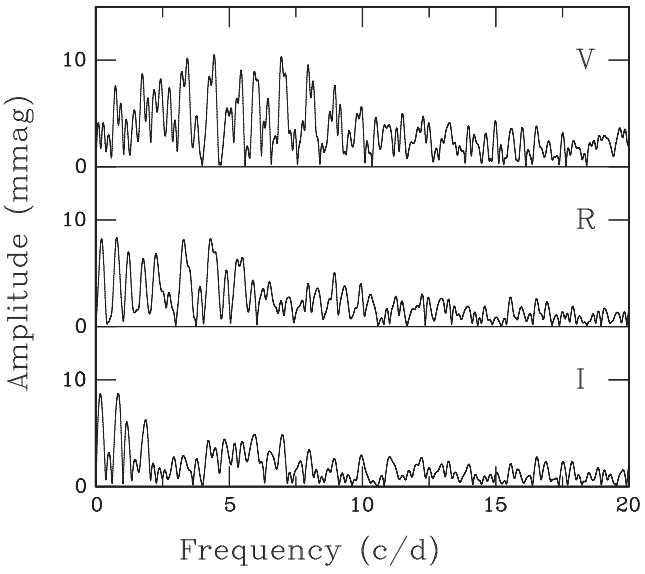

Figure 6. Amplitude spectra of the residuals left after pre-whitening the most prominent frequency (as given in the first line of Table 3) from the observations plotted in Figs 2–4.

Table 3. The results of successive pre-whitening of the SAAO data. Frequencies extracted from the *V*-filter data are listed in the order in which they were obtained. For the other two filters the closest matches (bearing in mind aliasing) are shown. Formal (least-squares) errors are given in brackets.

V		*R*		*I*	
Frequency (d^{-1})	Amplitude (mmag)	Frequency (d^{-1})	Amplitude (mmag)	Frequency (d^{-1})	Amplitude (mmag)
3.994 (0.004)	34.2 (1.5)	2.996 (0.003)	30.6 (1.0)	4.005 (0.005)	15.9 (0.8)
4.442 (0.011)	11.3 (1.4)	4.457 (0.009)	7.7 (0.7)	5.469 (0.013)	4.2 (0.6)
6.971 (0.010)	10.6 (1.2)	4.944 (0.010)	5.0 (0.6)	7.047 (0.012)	4.7 (0.6)
3.192 (0.013)	7.1 (1.1)	3.223 (0.008)	7.1 (0.6)	4.207 (0.013)	3.8 (0.5)
1.748 (0.018)	4.8 (1.0)	0.785 (0.009)	8.1 (0.9)	0.840 (0.007)	8.2 (0.7)

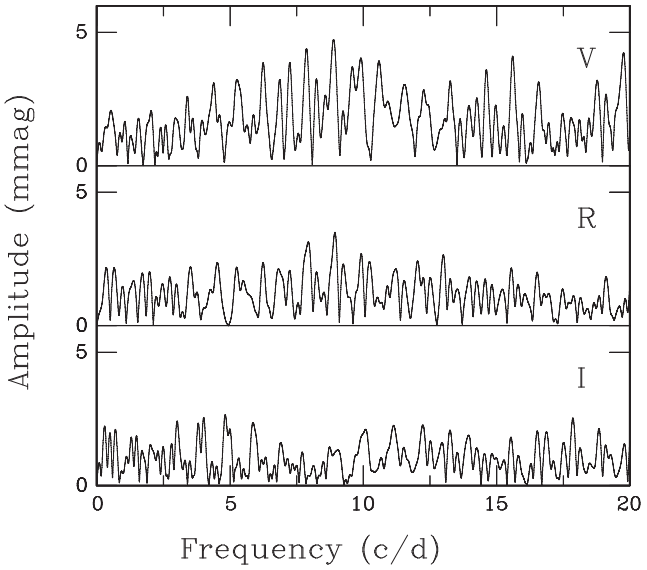

Figure 7. Amplitude spectra of the residuals after pre-whitening five frequencies (see Table 3) from the observations in Figs 2–4.

The fitted frequencies and amplitudes are listed in Table 3. The *V*-filter frequencies were obtained in the order listed. In the case of *R* and *I*, an attempt has been made to match 1 d^{-1} aliases to the *V*-filter frequencies. The interpretation of entries in Table 3 is aided by study of the PTF photometry, which follows.

4 FREQUENCY ANALYSIS OF THE PTF PHOTOMETRY

The PTF photometry of CVSO 30 was very kindly made available to the author by Dr. Julian Van Eyken. Observations were made through an *R* filter, in two blocks of 43.1 d ($N = 3430$) and 9.1 d ($N = 1903$), with a gap of almost a year (327 d) between them. For convenience the two sets of data will be referred to as the '2009' and '2010' data, respectively. Measurements with estimated errors in excess of 0.05 mag were discarded, leaving 3393 and 1900 values, respectively, for the two seasons.

Since the gap between the two data sets is quite long, these were analysed separately. Amplitude spectra are plotted in Figs 8 and 9. The top panels of the two graphs show the spectra of the raw data from the two seasons. The superior frequency resolution of the longer 2009 data set is evident, as is the fact that the amplitude of variability was considerably larger in the earlier data. The largest peaks none the less occur at the same frequency, $f_1 = 3.004$ d^{-1} (see the first line of Table 4).

Pre-whitening f_1 from the data leads to the spectra in the second panels of Figs 8 and 9. The amplitudes associated with the two largest peaks are close, but the frequencies f_2, although similar at 2.231 and 2.42 d^{-1}, differ by many formal standard errors.

Further evidence that the difference between the 2009 and 2010 values of f_2 is real comes from the frequencies in lines 4 and 5 of Table 4, which are evidently harmonics of f_2. For the 2009 data, $2 \times 2.2312 = 4.4624$, $3 \times 2.2312 \approx 6.694$ d^{-1} which are very close to 4.4616 and 6.690 d^{-1} in the table. Similarly, for the 2010 data, $2 \times 2.242 = 4.484$, $3 \times 2.242 = 6.726$ d^{-1}, close to 4.472 and 6.715 d^{-1} in the table.

Inspection of Table 4 reveals good agreement between the sets of first five frequencies extracted from either data set, if allowance is made for aliasing. The last panel of Fig. 8 suggests that essentially

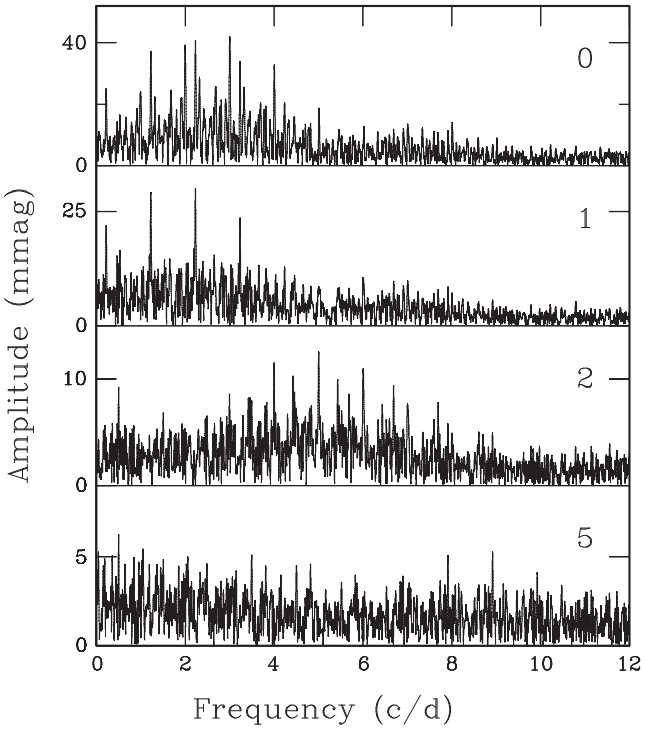

Figure 8. Amplitude spectra of the PTF 2009 data. Panels are labelled with the number of sinusoids which have been pre-whitened from the data. Note the different vertical scales on the different panels.

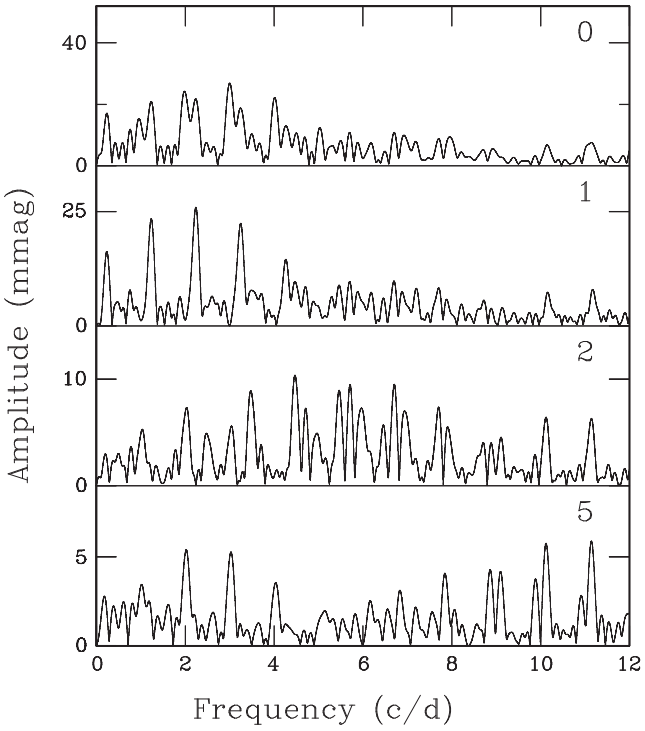

Figure 9. Amplitude spectra of the PTF 2010 data. Panels are labelled with the number of sinusoids which have been pre-whitened from the data. Note the different vertical scales on the different panels.

Table 4. The results of successive pre-whitening of the two sets of PTF observations. Frequencies extracted from the 2009 data set are listed in the order in which they were obtained. For the 2010 data set matches (bearing in mind aliasing) are shown. Formal (least-squares) errors are given in brackets.

2009		2010	
Frequency (d^{-1})	Amplitude (mmag)	Frequency (d^{-1})	Amplitude (mmag)
3.0039 (0.0002)	42.3 (0.8)	3.004 (0.002)	27.6 (0.8)
2.2312 (0.0003)	29.8 (0.6)	2.242 (0.001)	25.0 (0.5)
5.0061 (0.0006)	13.1 (0.6)	5.997 (0.003)	7.7 (0.4)
4.4616 (0.0007)	10.0 (0.6)	4.472 (0.003)	9.8 (0.4)
6.6898 (0.0010)	6.9 (0.6)	6.715 (0.003)	8.4 (0.4)

all the 2009 data set signal information is contained in these frequencies, and that pre-whitening these leaves pure noise. The residual spectrum in the bottom panel of Fig. 9, on the other hand, implies that there is further frequencies to be extracted from the 2010 data, but this is not pursued, as there are no obvious counterparts in the 2009 data set.

An obvious interpretation of the 2010 frequency 5.997 d^{-1} is that it is the first harmonic of the dominant $f_1 = 3$ d^{-1}. Similarly, the 2009 frequency 5.006 d^{-1} can be interpreted as a 1 d^{-1} alias of a 6 d^{-1}, again the first harmonic of f_1.

In summary, the data from both seasons are dominated by two non-sinusoidal signals, with fundamental frequencies of 3 and 2.23–2.24 d^{-1}. The first of these frequencies is quite stable, though the amplitude changed dramatically between the two observing seasons. The second frequency may not be stable, but its amplitude (and even those of its harmonics) appears to have remained unchanged from the first season to the second.

5 FREQUENCY ANALYSIS OF THE CATALINA PHOTOMETRY

The Catalina Sky Survey for objects moving rapidly through the night sky has made available time series photometry of millions of stars, with the second data release covering 7 yr. No filters are used, in order to maximize count rates. In the case of CVSO 30, 329 measurements are available. One outlying observation with an estimated error of 0.08 mag was rejected; with the exception of four data points with 0.07 mag errors, all other errors are placed at 0.06 mag. Magnitudes are recorded to the nearest 0.01 mag.

Amplitude spectra of the CSS data are plotted in Fig. 10. The highest peak in the top panel is at a frequency of 2.003 17 d^{-1}, with a formal standard error of only 2×10^{-5} d^{-1}. Pre-whitening leads to the spectrum in the middle panel of the figure, with the largest peak at $f = 1.227\,43$ d^{-1}, again with a standard error of 2×10^{-5} d^{-1}. These are evidently 1 d^{-1} aliases of f_1 and f_2 defined above.

Comparison of Fig. 10 to Figs 8 and 9 shows that while the amplitudes of the $f_2 = 2.23$ d^{-1} variation is similar in all three cases, the f_1 variation has a much lower amplitude in Fig. 10. Material in the preceding section already suggested that the amplitude associated with f_1 is variable – Fig. 10 reinforces this.

6 DISCUSSION

The picture to emerge from the previous two sections of the paper is that CVSO 30 varies non-sinusoidally with two periods. The fundamental frequencies are $f_1 \approx 3$ (or perhaps 2) d^{-1} and $f_2 \approx 2.23$ d^{-1}, the latter corresponding to the value identified by Van Eyken et al.

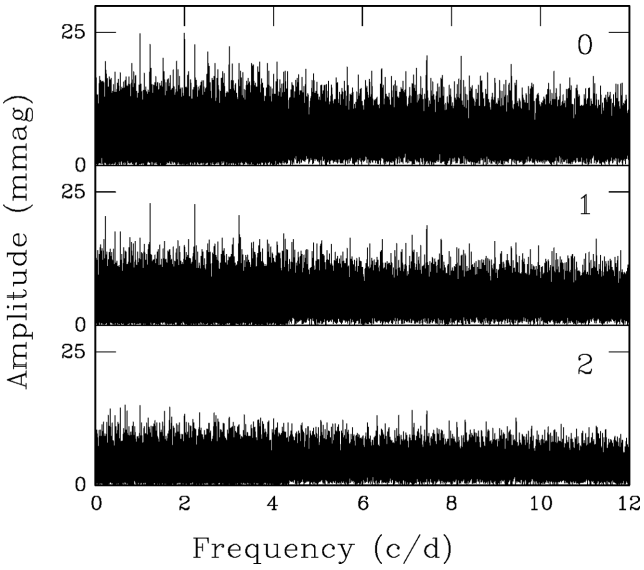

Figure 10. Amplitude spectra of Catalina survey data. Panels are labelled with the number of pre-whitened sinusoids.

(2012). Returning to the SAAO data, in particular Table 3, it is possible to interpret the frequencies in the first line as corresponding to f_1 (or its 1 d^{-1} aliases), with first harmonics (or 1 d^{-1} aliases thereof) of f_1 in the third line. The second line of Table 3 corresponds to the first harmonic of f_2 (or its 1 d^{-1} alias, in the case of the *I* filter). The fourth line of Table 3 has 1 d^{-1} aliases of f_2 (*V* and *R*) or a 2 d^{-1} alias of f_2 (*I*). It is only the low frequencies in the last line of the table which have no counterparts in Table 4 or in the CSS data: these may be due to imperfect standardization, based on just a few stars in the field of view of the SAAO camera.

The amplitude of f_1 observed in *R* in 2015 (SAAO data) is very similar to that seen in the 2010 PTF data (31 versus 28 mmag). However, both the amplitude, and the shape, of the f_2 variation has changed substantially: in the more recent (SAAO) data the amplitude is only about a third of that seen in the PTF observations, and it is dominated by the first harmonic. In fact, the only property of the light curve which appears to remain unchanged over time is the frequency f_1.

If f_1 and its first harmonic are pre-whitened from the PTF data, and the residuals folded with respect to f_2, Fig. 11 is obtained. Phase-folding in the top two panels is with respect to the respective best-fitting values of f_2. In the bottom panel of the figure the 2010 data have been folded with respect to f_2 determined from the 2009 data, as this more clearly illustrates the presence of the light-curve dips which may be due to transits. Note though, that it is not only the dips which are periodic – the entire folded light curve repeats with a period of $1/f_2$ d.

Periodic light-curve shapes such as those in Fig. 11 are not impossible in WTTSs – see for example the MOST ('Microvariability and Oscillations of Stars') satellite photometry of four WTTSs in Siwak et al. 2011, or synthetic light curves in Walkowicz, Basri & Valenti (2013). However, the presence of two apparently independent and unrelated periodicities f_1 and f_2 at first glance appears to pose a problem for models based on rotational modulation. Spots at different latitudes, with different surface rotation speeds, is one way of solving this conundrum: for example, the correct f_1 alias could be 2 d^{-1}, so that the required differential rotation frequency range would be $\Delta f \approx f_2 - f_1 = 0.23$ d^{-1}.

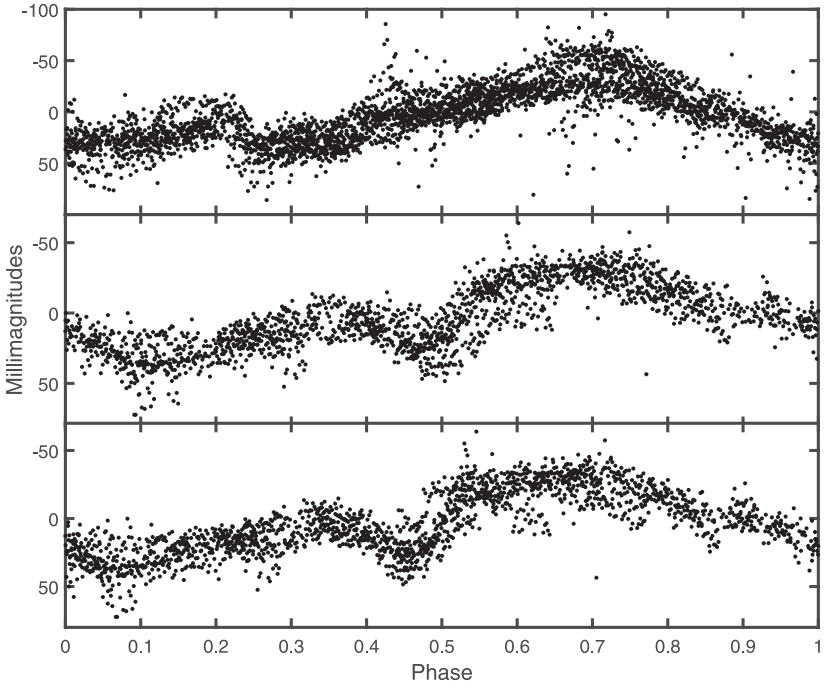

Figure 11. Top panel: pre-whitened PTF 2009 data, folded with respect to a period of 1/2.2312 d. Middle panel: pre-whitened PTF 2010 data, folded with respect to a period of 1/2.242 d. Bottom panel : pre-whitened PTF 2010 data, folded with respect to a period of 1/2.2312 d. Pre-whitening consisted of removing f_1 and its first harmonic.

Barnes et al. (2005) provide a summary study of observational differential rotation research in spotted stars. Two pertinent findings in their paper are that differential rotation declines with decreasing effective temperature, but increases with rotational velocity. The latter effect can be quantified from their fig. 3 as

$$\Delta f = 0.0094 f^{0.15}, \quad (1)$$

where the rotation period is $1/f$. The relation (1) implies $\Delta f \approx 0.01$ d^{-1} for f in the range 1–3 d^{-1}. This is an order of magnitude smaller than the range required to explain periodicities in CVSO 30. Note though that with observed equatorial and polar solar rotation periods of, respectively, ∼25 and ∼35 d (e.g. Hathaway, Upton & Colegrove 2013), $\Delta f/f = 0.364$ in the sun, so that the required value of 0.11 for CVSO 30 may not be preposterous.

It is interesting to consider the qualitative implications of the *VRI* amplitudes listed in Table 3 for star-spot temperatures and filling factors. The simple two-temperature approximation described in Stahler & Palla (2004) is sufficient for this purpose:

$$\Delta m_\lambda \approx \pm 2.5 \log \left\{ 1 - \kappa \left[1 - \frac{B_\lambda(T_{\rm spot})}{B_\lambda(T_{\rm star})} \right] \right\},$$

where Δm_λ is the peak-to-peak amplitude at wavelength λ, κ is the filling factor (fraction of the facing hemisphere covered by the star-spot), $T_{\rm star}$ and $T_{\rm spot}$ are the stellar and spot effective temperatures, and $B_\lambda(T)$ is the flux at wavelength λ. The negative (positive) sign applies if the spot is cooler (hotter) than the stellar photosphere. Assuming blackbody radiation,

$$B_\lambda(T) = \left[\exp\left(\frac{\alpha}{\lambda T} \right) - 1 \right]^{-1} \qquad \alpha = 1.44 \times 10^8 \text{ Å K}.$$

In what follows $T_{\rm star} = 3470$ K is adopted from Briceño et al. (2005).

Since there are data for three filters (i.e. three values of λ), but only two unknowns (κ and $T_{\rm spot}$) solutions are obtained by minimizing

$$SS(\kappa, T_{\rm spot}) = \sum_\lambda [\Delta m_\lambda(\text{observed}) - \Delta m_\lambda(\text{predicted})]^2 .$$

Plausible solutions, listed in Table 5, could only be obtained for hot star-spots. Very small filling factors are required to reproduce the relatively small variability amplitudes.

There is, of course, an observational objection to the hotspot model: as pointed out in the Introduction, there is no evidence for any infrared excess, and, by implication, no evidence for substantial amounts of circumstellar material. It is none the less conceivable that the required amount of accreted material may be small enough to be supplied by low-density hot circumstellar gas. An observational discriminant for the presence of such accretion is an ultraviolet, rather than infrared, excess (e.g. Herczeg, Cruz & Hillenbrand 2009).

7 CVSO 209

The star CVSO 209, classified as a WTTS by Briceño et al. (2007), is 1.6 arcmin to the north-east of CVSO 30. The spectral type of CVSO 209 is M3, and the Hα equivalent width 5.8 Å, from low-resolution spectroscopy. *Spitzer* photometry by Hernández et al. (2007) showed no infrared excess, and hence no evidence for a circumstellar disc.

Variability in CVSO 209 was discovered by the CSS (Drake et al. 2014). The period and amplitude were determined to be 0.936 d and 0.14 mag, and it was classified as a close eclipsing binary. Since the star was within the field of the SAAO CCD camera from night 2 onwards, the variability can be investigated in more detail – see Fig. 12 for the light curves.

Table 5. The results of modelling the peak-to-peak amplitudes of f_1 and f_2 in Table 3 in terms of (hot) star-spots. Model amplitudes Δm_λ are followed by the observed amplitudes, given in brackets. The quantity κ is the filling factor, and $\sqrt{SS}$ is an estimate of the residual scatter.

Frequency (d^{-1})	Temperature (K)	κ	Δm_V (mmag)	Δm_R (mmag)	Δm_I (mmag)	$\sqrt{SS}$ (mmag)
f_1	4410	0.017	71 (68)	53 (62)	38 (32)	11
f_2	5560	0.0013	23 (22)	15 (15)	9 (8)	1.2

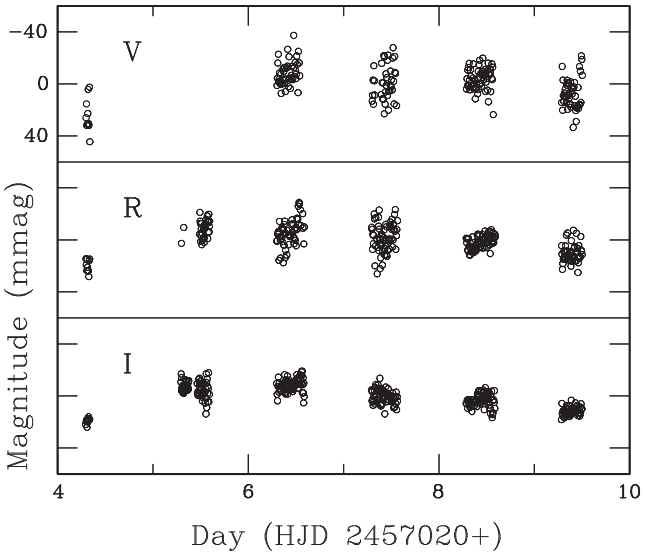

Figure 12. The SAAO photometry of the WTTS CVSO 209. The star is ∼0.6 mag fainter than CVSO 30 in the *V* band, which accounts for the noisy *VR* measurements.

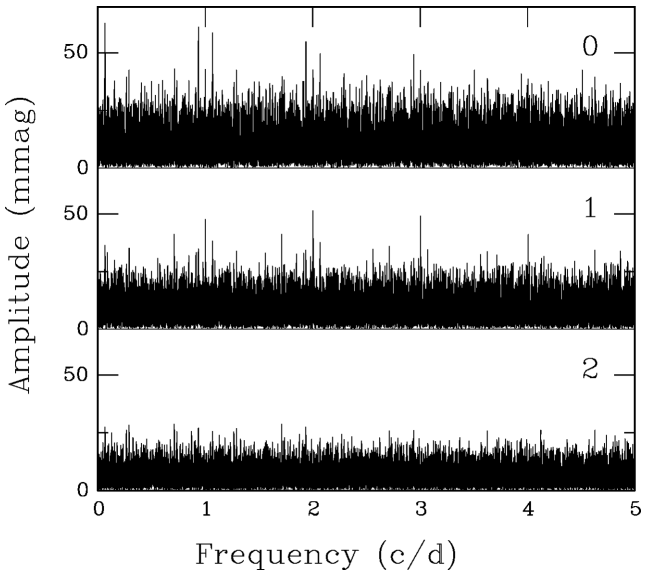

Figure 13. Spectra of the CSS photometry of CVSO 209. Panels are labelled with the number of pre-whitened sinusoids.

The characteristics of the Catalina photometry of CVSO 209 are quite similar to those of the CVSO 30 measurements. Discarding six observations with large estimated errors leaves a data set of length 324. Amplitude spectra can be seen in Fig. 13. The highest peaks in the top and middle panels are at frequencies 0.06512 ($\pm 1 \times 10^{-5}$) and 2.00252 ($\pm 1 \times 10^{-5}$) d^{-1}, with amplitudes of 69 and 50 mmag. There is no evidence for systematic intranight variability in the SAAO data, indicating that the latter frequency is an artefact. This is confirmed by plotting the residual light curve (i.e. after pre-whitening by the 0.065 12 d^{-1} frequency): it shows a long-term trend, suggesting that $f \approx 2$ d^{-1} is the 2 d^{-1} alias of a frequency near zero. Pre-whitening the residual light curve by subtraction of a fitted quadratic in fact removes peaks near multiples of 1 d^{-1}, i.e. the signal content of the CVSO 209 data consists of a quadratic trend and a 0.06512 d^{-1} sinusoid.

The frequency of 0.065 12 d^{-1} corresponds to a period of 15.356 d, which is not overtly inconsistent with the light curves in Fig. 12. If the periodicity is due to rotation, it is towards the upper end of the range seen for young, low-mass stars (e.g. Moraux et al. 2013).

8 CONCLUSIONS

Regardless of whether CVSO 30 has a planetary companion, it is an interesting star. Fig. 11 suggests that the dips in the light curve may be just part of a complicated non-sinusoidal periodicity in the object. In this respect it may resemble the short period WTTS CD-36 3202, in which a similar depression in the light curve has been observed (Koen 2015). It is also noteworthy that Stauffer et al. (2015) have discovered periodic dips in the light curves of several classical T Tauri stars, ages of which are similar to that of CVSO 30. In cases where the stellar rotation periods are known, it turns out that these are equal to the dip periods – as is the case with CVSO 30. The origin of the dips is thought to be extinction by cool corotating clumps of dust.

If the dips are indeed due to planetary transits, then precession of the orbit of the planet could explain the temporary absence of transits (Barnes et al. 2013).

There is also a second non-sinusoidal signal in the data. It is not clear if the two periodicities are driven by the same mechanism – if both are due to rotation, then differential rotation in CVSO 30 is more extreme than usually seen in stars (the sun aside). In order to make progress with modelling of the periodicities it is essential that the aliasing ambiguity be resolved. This can be accomplished by suitable multisite photometric monitoring of the star. Photometry or low-dispersion spectroscopy in the ultraviolet might reveal whether there is accretion on to CVSO 30, which would provide evidence for or against hot star-spots.

It is perhaps also worth mentioning that two apparently unrelated periods have been detected in the K3 T Tauri star UNSW V760 (e.g. Koen et al. 2013). The authors speculate that the latter star may be in a short-lived phase during which pulsations can be excited.

ACKNOWLEDGEMENTS

The author is grateful to Dr Julian Van Eyken who graciously shared the photometry of CVSO 30 discussed in Van Eyken et al. (2012). The author also thanks those maintaining the SIMBAD data base in Strasbourg, France; the CSS for public access to their photometry; the South African National Research Foundation for financial support; and the SAAO for telescope time.

REFERENCES

Barnes J. R., Collier Cameron A., Donati J.-F., James D. J., Marsden S. C., Petit P., 2005, MNRAS, 357, L1
Barnes J. W., Van Eyken J. C., Jackson B. K., Ciardi D. R., Fortney J. J., 2013, ApJ, 774, 53
Briceño C., Calvet N., Hernández J., Vivas A. K., Hartmann L., Downes J. J., Berlind P., 2005, AJ, 129, 907
Briceño C., Hartmann L., Hernández J., Calvet N., Vivas A. K., Furesz G., Szentgyorgyi A., 2007, ApJ, 661, 1119
Drake A. J. et al., 2014, ApJS, 213, 9
Errmann R., Raetz St., Kitze M., Neuhäuser R., the YETI team, 2014, Contrib. Astron. Obs. Skalnaté Pleso, 43, 1
Hathaway D. H., Upton L., Colegrove O., 2013, Science, 342, 1217
Herczeg G. J., Cruz K. L., Hillenbrand L. A., 2009, ApJ, 696, 1589
Hernández J. et al., 2007, ApJ, 671, 1784
Koen C., 2015, MNRAS, 449, 1704
Koen C., Gray R. O., Kawaler S., Crawford S. M., 2013, MNRAS, 435, 2494
Moraux E. et al., 2013, A&A, 560, 13
Schechter P. L., Mateo M., Saha A., 1993, PASP, 105, 1342
Siwak M., Rucinski S. M., Matthews J., Kuschnig R., Guenther D. B., Moffat A., Sasselov D., Weiss W. W., 2011, MNRAS, 415, 1119
Stahler S. W., Palla F., 2004, The Formation of Stars. Wiley-VCH, Weinheim
Stauffer J. et al., 2015, AJ, 149, 130
Van Eyken J. C. et al., 2012, ApJ, 755, 42
Walkowicz L. M., Basri G., Valenti J. A., 2013, ApJS, 205, 17

SUPPORTING INFORMATION

Additional supporting information may be found in the online version of this article:

vri
(http://mnras.oxfordjournals.org/lookup/suppl/doi:10.1093/mnras/stv906/-/DC1).

Please note: Oxford University Press are not responsible for the content or functionality of any supporting materials supplied by the authors. Any queries (other than missing material) should be directed to the corresponding author for the article.

This paper has been typeset from a TEX/LATEX file prepared by the author.